Advances in Environmental Technology 4 (2022) 311-327

Iranian Reasearch Organization for Science and Technology (IROST)

Advances in Environmental Technology

Journal home page: https://aet.irost.ir/

Raw and treated Avokado waste to remove Bemacid Red-ETL dye from aqueous solution: kinetics and theoretical physics modeling

Ouazani Fouzia[1*], Benhammadi Samia[2], Iddou Abdelkader[3]

[1]Energy and process engineering department, Faculty of Technology, Sidi Bel Abbes, Algeria

[2]Laboratory of Science, Technology and Process Engineering-LSTGP. University of Science and Technology USTO- Oran, Algeria

[3]Laboratoire des Ressources Naturelles Sahariennes. Faculté des sciences et de la technologie, Université Ahmed Draia – Adrar, Algeria

ARTICLE INFO

Document Type:
Research Paper

Article history:
Received 31 July 2022
Received in revised form
28 September 2022
Accepted 1 October 2022

Keywords:
Bemacid Red
Kinetic models
Theoretical physic models
Adsorption
Wastewater treatment.

ABSTRACT

The raw and modified surface of agricultural waste of Avokado was investigated in the adsorption of textile dye Bemacid Red. Phosphoric Acid, sodium hydroxide, and Acetone were used to treat the adsorbent surface. Batch mode studied the effects of experimental parameters: solution pH, contact time, initial dye concentration and temperature. The fit of the kinetics data was performed by the pseudo-first and second-order models. Whereas the adsorption isotherm data was performed by the statistical physics models. The Batch results reveals that the contact time and initial concentration have a positive effect on adsorption capacity, however, the two other parameters have a negative effect. From the kinetic modeling results, it was observed that the pseudo-second order fit well the data with a height determination coefficient ($0.971< R^2 < 0.984$). On the other side the double layer with two energies from the tested physical models proves to be the best model to explain the Bemacid Red dye adsorption mechanism ($0.0991<R^2<0.999$ for the raw and treated Avokado). The modeling analysis indicated that dye molecules occurred via parallel orientation onto raw and NaOH-treated Avokado at 20 °C and via non-parallel orientation at temperature greater than 20 °C. In summary the NaOH-treated Avokado gives an important affinity towards Bemacid Red dye and can be classified as a low and efficient adsorbent.

1. Introduction

A low amount of fresh water is accessible to human use (less than 3%) [1]. However, this amount of water has recognized a decrease because of the rapid advent of urbanization and industrialization. The accumulation of persistent pollutants in the water stream due to the uncontrolled discharge of municipal, domestic and industrial wastes in ecosystem, significantly poses a harmful effect on

*Corresponding author: Tel: 0772662024
E-mail: ouazanifouzia@yahoo.fr
DOI:10.22104/AET.2022.5782.1587

the environment and human health [2]. The textile industry is the main factor of water and environment pollution, where the annual production of synthesized dyes recognized a significant increase in the order of 8.105 tons per year, which are mainly applied in the paper, textile, food, cosmetic, leather, plastic and pharmaceutical industries, etc [3]. A large percentage of synthesized dyes is directly discharged in ecosystem without any pre-treatment. These discharged dyes easily enter the food cycle and causes severe sanitary risk by her carcinogenic metabolites. The main need is to find powerful techniques for the recycling and reuse of the textile industry wastewater. Different physicochemical conventional techniques are applied in the treatment of colored wastewater [4]. However, the applications of certain treatment techniques generate a large amount of chemical sludge and more toxic by-products or are ineffective treatments in the removal of various dyes comparing to the cost of the process [5]. Adsorption and because of its remarkable efficiency when treating the wastewater of the textile industry, recognized considerable interest in adapting it as an effective technique compared to the application of other conventional techniques [6]. In order to solve these problems, various efforts have been made to raise the efficiency of treatment and minimize regeneration of toxic chemicals by-products [7]. However, from industrial and economic standpoint the application of any treatment techniques obeyed through an analysis of the treatment efficiency in parallel to the expenditure involved in the process. These expenditures pushed researchers to elaborate inexpensive potentially renewable adsorbents of various available materials. To solve these environmental problems, there are different ecofriendly treatment methods. Among these treatments, there is the degradation of pollutants by photocatalysis which consists to decompose the pollutants so as to reduce their toxicity [8-9]. There is also the adsorption which is based on the number of the active sites present on the adsorbent surface able to fix the maximum of polluting molecules [10]. In this context, several researches were designed to develop new composites that will be used either to degrade organic pollutants or either to increase their adsorption affinity towards these pollutants [11-13]. In the same context, the biosorbents continues to be among the less expensive alternative adsorbents applied in separation techniques of organic or inorganic pollutants [14]. Avokado is one of high nutritional fruits, the consumption of this fruit increased up to 5.6% per year [15]. Therefore, there is considerably high abundant waste from human and food processing [16]. For these reasons in this work the Avokado is used as adsorbent. The aim of the present work is to investigate the biosorption capacity of Avokado waste (peel and nut) to remove Bemacid Red from aqueous solution. The adsorbent was tested at raw and treated aspect to remove dye. The characteristics of raw and treated Avokado were evaluated by Scanning Electron Microscope (SEM), Fourier Transform Infrared (FTIR) spectroscopy analysis and X-ray fluorescence spectra (ED-XRF). In batch mode, the effects of some operating conditions including initial dye concentration, contact time, medium pH and temperature on the dye sorption were investigated. Kinetic and physical theoretical models of the biosorption processes were analyzed in terms of the pseudo-first order, pseudo-second order models, monolayer with single energy and double layer with two energies models, respectively. Also, the aim is understand Bemacid Red dye adsorption mechanism and the fixing way of dye molecules onto the adsorbent surface. And to find the treatment type that improves the Avokado adsorption capacity.

2. Material and methods

2.1. Adsorbent collect and treatment

Avokado waste (peel/nut - AWPN): was provided from local commerce as fruit, the Avokado waste (peel/nut) was washed with distilled water, and then dried in oven at 80°C for 24 h. The dried mass was grind into fine particle of average diameter of 250 μm. Bemacid Red is among ETL family dyes, is an acidic dye; marketed by BEZMA Dye Company and is most used the in textile industry in Algeria with unknown chemical structure. All chemicals and reagents used in this study were of analytical grade. Sodium hydroxide (NaOH, 98%) is purchased from Sigma-Aldrich. Whereas, Acetone (C_3H_6O, 99%), phosphoric acid (H_3PO_4, 97%) and

nitric acid (HNO_3) were purchased from Biochem Chemopharma. Distilled water was employed throughout the experiments.

2.2. Organic and inorganic impregnation

For inorganic impregnation the using method was described by Tezcan et al. [17], 5 g of precursor (AWPN) was mixed with 250 mL of NaOH (1M) under agitation 340 rpm; the impregnation process duration was 24 h. After impregnation the sample was filtered and washed several times with distilled water up to the total elimination of the base excess used in this treatment (until pH = 6.7). The same steps with the same conditions were used for the impregnation by H_3PO_4.The two samples were dried in oven at 50 °C for 24 h. the acidic and basic treatment samples were labeled AWPNA and AWPNB respectively and the raw precursor was labeled AWPNBr. For organic impregnation [17], 5 g of the biosorbent was mixed with 50 mL of acetone (C_3H_6O) under agitation speed of 340 rpm. The impregnation process was stopped after 6h. The sample was washed several times with distilled water up to remove the acetone excess. The sample was dried in oven for 24 h at 50 °C. The sample was labeled AWPNAc.

2.3. Characterization of treated adsorbents

To test these different samples in the field of water treatment requires determination of their physicochemical properties in order to explain the phenomena that govern the efficiency and the adsorption capacity of the used supports. pH_{pzc} using the method described by Pashai et al. [18], Scanning Electron Microscopy (SEM), FTIR analysis and Energy dispersive X-ray fluorescence (ED-XRF) analysis were performed.

2.4. Batch adsorption experiments

Batch adsorption was studied to determine the removal efficiency of Bemacid Red dye from different operating conditions (pH medium from 1 to 9, initial dyes concentration from 5 mg/L to 800 mg/L, contact time from 5 min to 60 min and temperature from 20°C to 50°C). Amount of 50 mg of adsorbent was mixed with 50 mL of Bemacid Red dye solution under agitated at 340 rpm for selected interval time. The desired pH value was adjusted by adding NaOH (0.1M /0.01M) or HNO_3 (0.1M / 0.01M) using pH-meter (SCHOTT CG711). Then the mixture was filtered to separate the sample from the aqueous phase. The residual amount of Bemacid Red dye is determined by spectrophotometer analysis UV-Visible (HACH DR 2000) at 500 nm. The four samples (AWPNB, AWPNA, AWPNBr and AWPNAc) are tested under the same experimental conditions. The adsorption capacity q_e(mg/g) is calculated through the following formula Eq (1) [19]:

$$q_e = \frac{C_0 - C_e}{m} V \quad (1)$$

Where c_0 is the initial dye concentration (mg/L) at t=0min and c_e is the equilibrium dye concentration at time t, V is the dye solution volume (L), and m is the mass (g) of the adsorbent. The percentage R% of dye removal from samples solution was calculated by the following equations Eq (2) [19]:

$$R(\%) = \frac{(C_0 - C_e)}{C_0} \times 100 \quad (2)$$

3. Results and discussion

3.1. Characterization results

3.1.1. pH_{pzc} of different adsorbent

The pH_{pzc} of each adsorbent is an important factor helps to explain the behavior of the adsorbent surface load in aqueous solutions. The method used consists to mixed a determined amount of each adsorbent with a 50 ml NaCl solution (10%) and the intersection between initial pH_i (at t=0h) according to the final pH_f (at t =24 h) represent the adsorbents pH_{pzc}. The obtained pH_{pzc} values (**Fig.1**) of the different adsorbents are: 5.5, 4.2, 3.1 and 7.7 for AWPNBr, AWPNAc, AWPNA and AWPNB respectively. At these values, the adsorbent surfaces have a neutral charge. That means for solution pH under pH_{pzc} values the adsorbent surface charge becomes positive and this helps to eliminate molecules which have functional groups with negative charge. And in the opposite case the load of the surface of the adsorbent becomes negative which helps to attach molecules which contain functional groups with positive charge. The four tested samples have different pH_{pzc}, this difference can be explained by the treatment effect on the adsorbent surface as well as the change in functional groups and their charge. The obtained values of pH_{pzc} are compared with other research, when the pine bark compost

and municipal solid waste compost are used as adsorbent to remove Basic Violet 10 (BV10) and Acid Red 27 (AR27) dyes by Khaled et al. [20] the pH_{pzc} were found to be 4.4 and 8.2 respectively.

3.1.2. Effect of dosage

Fourier Transform Infrared Spectroscopy (FTIR) of the raw and treated adsorbent are shown in Figure 2. In the four Spectrums, the peaks observed at 3480 cm^{-1} are related to the hydroxyl (O-H) group [21] Aliphatic C–H stretching is situated at 2980 cm^{-1} [22]. The presence of C=O of the carboxylic acids of hemicelluloses is observed at 1780 cm^{-1} [23]. The two peaks around 1670 cm^{-1} and 1350 cm^{-1} are related to alkenyl C=C and COO^- symmetric stretching vibration [24]. The bands at 1120 cm^{-1} are attributed to the C–O stretching of ether group [25]. It was seen that the NaOH treatment caused some changes in the AWPNB spectrum, compared to others spectra where some peaks have become wider. The morphology of AWPNBr, AWPNAc, AWPNA and AWPNB are shown in Figure 3, by SEM micrographs taken. It is clear that the surfaces of the four supports were not smooth, but contains cavities.

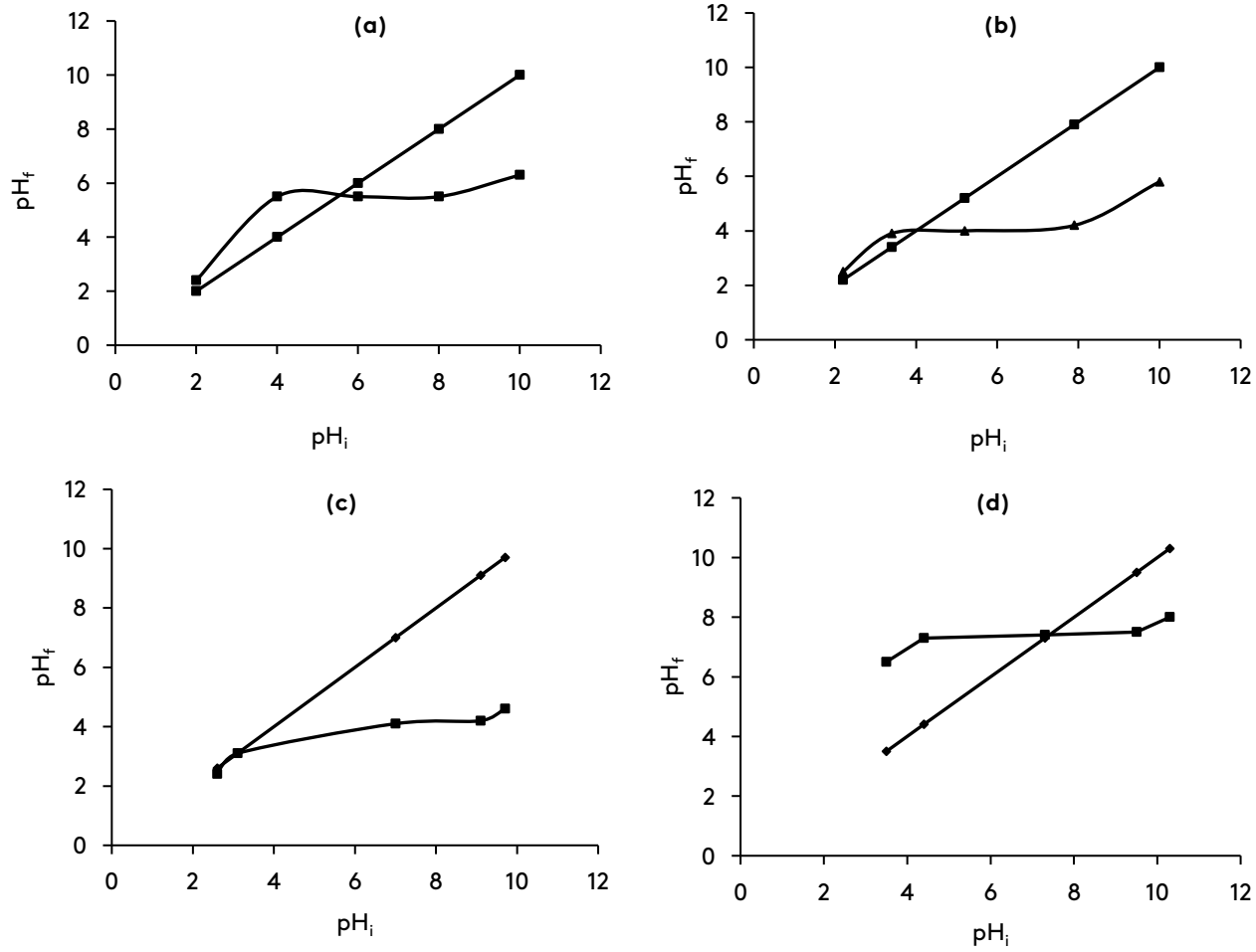

Fig.1. pH_{pzc} determination of different adsorbents: (a) AWPNBr (b) AWPNAc (c) AWPNA (d) AWPNB adsorbents.

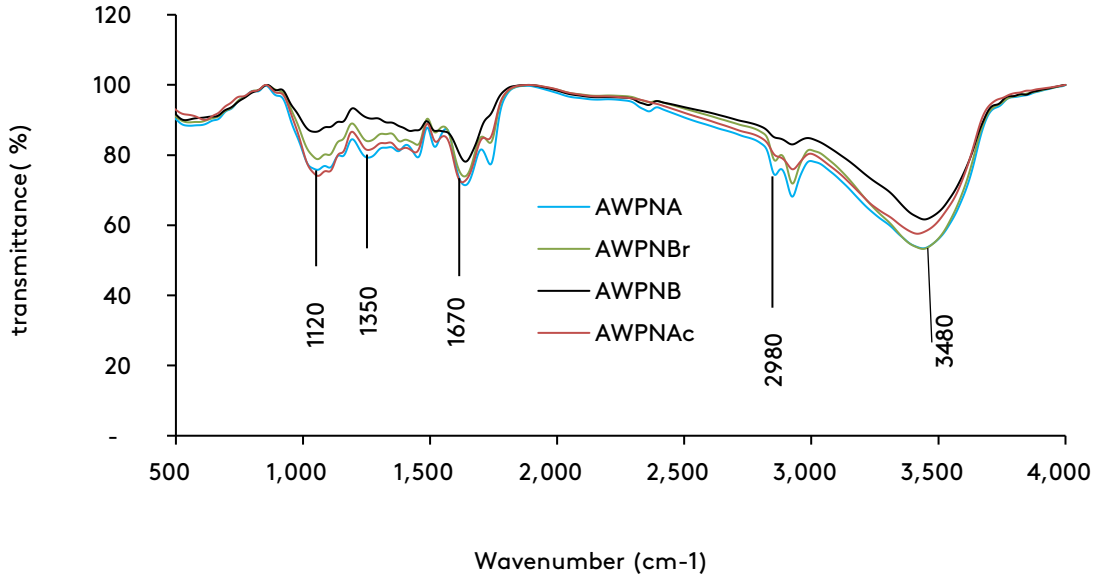

Fig.2. FTIR spectra of different adsorbents.

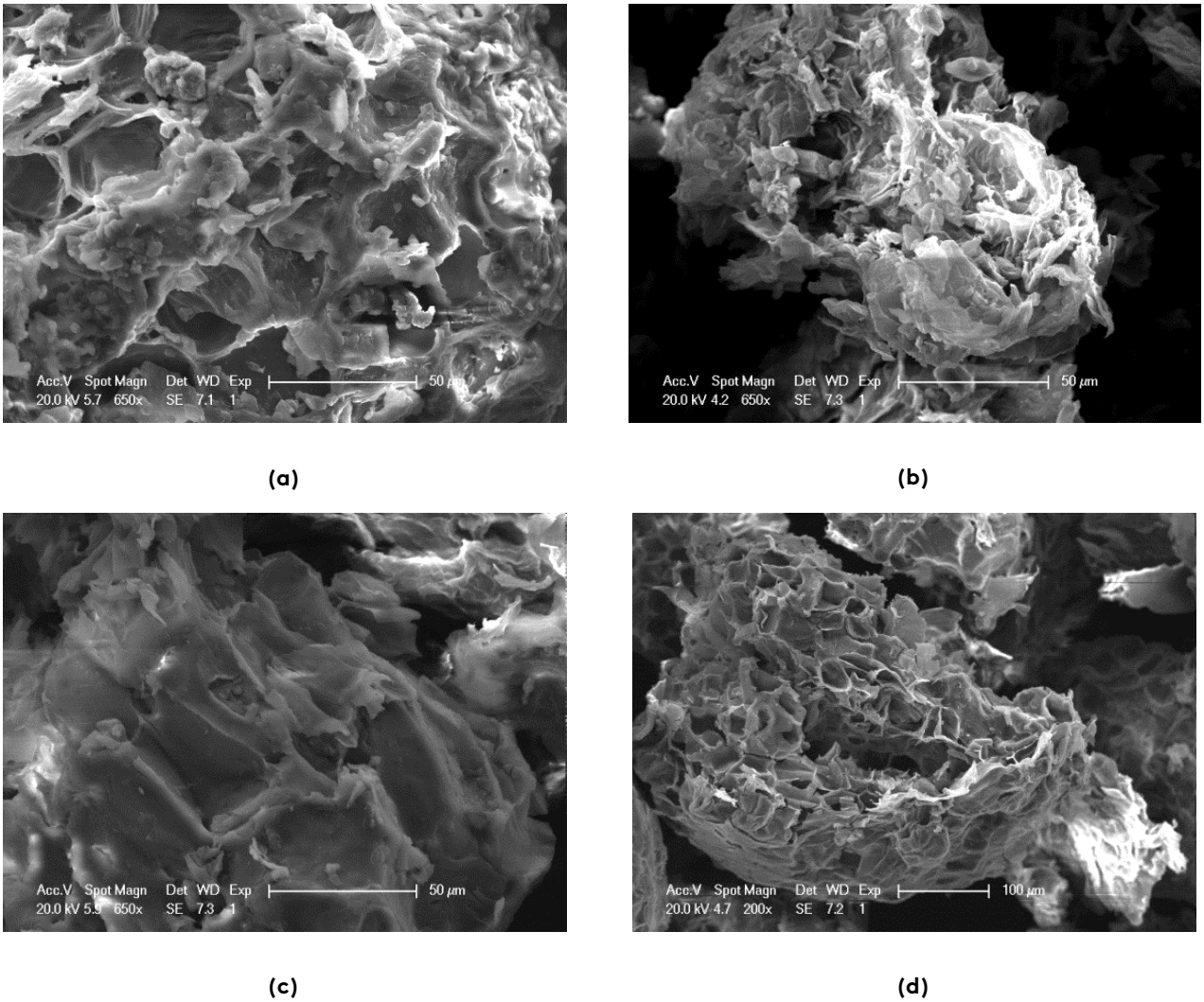

Fig.3. SEM micrographs of (a) AWPNBr, (b) AWPNAc, (c) AWPNA and (d) AWPNB.

3.1.3. ED-XRF analysis

Energy dispersive X-ray fluorescence (ED-XRF) spectrometer from Bruker equipped with a Rhodium X-ray tube and X-Flash® SDD detector is used to determine the chemical composition of different supports. The obtained results are listed in Table.1. The ED-XRF gives a description of the elemental composition of the inorganic constituents of the different adsorbent contributed to its ash composition. The results obtained from Table .1 indicates that the Calcium (Ca) with 1.38% is the major inorganic constituents of AWPNB, and in second position the AWPNBr at 0.6%, while Chloride (Cl), Nickel (Ni), Copper (Cu), Zinc (Zn), Lead (Pb) were abundant constituents at 0.035%, 0.0024%, 0.0014%, 0.0017%, 0.0008% respectively for AWPNBr adsorbent. Other constituents with trace composition for AWPNBr were: Titanium (Ti), Manganese (Mg), Iron (Fe), and Bromine (Br). In the case of AWPNA, there were only two constituents: calcium (Ca) and nickel (Ni) at 0.079% and 0.0022% respectively and all the other elements cited for the AWPNBr adsorbent, their compositions were in traces. For AWPNAc adsorbent, Chloride (Cl), Calcium (Ca), Nickel (Ni), Copper (Cu), Zinc (Zn) and Bromine (Br) were abundant constituents at 0.056%, 0.55%, 0.0025%, 0.0015% 0.001% and 0.0004% respectively and other elements their composition were in trace. For AWPNB, there were four elements their compositions were in traces: Chloride (Cl), Titanium (Ti), Manganese (Mg), and Iron (Fe). The obtained analysis results are in accordance with the previously reported results of element composition of biomass [26].

Inorganic treatment reduces the presence of Cl in the adsorbents structure of compared to organic treatment. On the other hand, the NaOH treatment increases the presence of Ca and which exceed the raw adsorbent values.

3.2. Effect of pH medium on Bemacid Red *dye removal*

Figure 4 shows the effect of pH on the R % adsorption of the four adsorbents towards Bemacid Red dye. The highest value of R% Bemacid Red removal was noted at an acidic pH =1 with 88% for AWPNB biomass. The minimum R% Bemacid Red adsorption of 48% was observed for AWPNA biomass at the same pH value. The decrease in R% of Bemacid Red adsorption was found with increase in pH range from 1 to 9. The obtained pH value (pH=1) was lower than the pH_{pzc} of each adsorbent that means that the adsorbent surface was positively charged. In addition, the Bemacid Red is an acidic dye which contains an anionic auxochrome group (fixing group). At the end of the adsorption process, the entire of adsorbent surface is colored, which means that the anionic auxochrome group was fixed on the surface of the different biomass. The Bemacid Red adsorption was favorable in acidic solution for the different tested biomass. At pH =1, the R% Bemacid Red removal by AWPNB is 2 times more than R% Bemacid Red removal by AWPNA. This may be due to difference in the presence of the function groups on the studied adsorbents (Figure 2) or may also be due to difference in the inorganic elements composition (Table.1). The R% Bemacid Red of the four tested adsorbents was following the order: R% (AWPNB) > R% (AWPNAc) > R% (AWPNBr) > R% (AWPNA). The pH =1 was the optimal solution condition of Bemacid Red dye removal for the different biomass and this value is used for the others conditions test. The suitable pH medium to eliminate Basic Violet 10 (BV10) and Acid Red 27 (AR27) are 5.3 and 8.5 respectively found by Khaled et al. [20] when they used compost of pin bark as adsorbent.

The effect of pH medium in the case of the photodegradation of methyl orange using SnO_2 as catalyst was important, where the degradation rate of this dye increases from 81% to 86% when the pH medium increases from 4 to 7 and decreases from 86 % to 63 % when the pH medium increases from 7 to 10. So, the optimum pH value in this case is 7 [23]. While the acidic medium is favorable for the photodegradation of the same dye (methyl orange) when other catalyst were applied as: MWCNTZN (pH = 4) [27], MWCNTS (pH = 3) [28]and MGOZ (pH = 3) [29].

Table.1. ED-XRF analysis of different adsorbents.

Name	Cl (%)	Ca (%)	Ti (%)	Mn(%)	Fe (%)	Ni (%)	Cu (%)	Zn (%)	Br (%)	Pb (%)
AWPNBr	0.035± 0.011	0.60± 0.02	< LOD	< LOD	< LOD	0.0024± 0.0007	0.0014± 0.0009	0.0017± 0.0004	< LOD	0.0008± 0.0008
AWPNA	< LOD	0.079± 0.009	< LOD	< LOD	< LOD	0.0022± 0.0007	< LOD	< LOD	< LOD	< LOD
AWPNA c	0.056± 0.012	0.55± 0.02	< LOD	< LOD	< LOD	0.0025± 0.0007	0.0015± 0.0009	0.0010± 0.0004	0.0004± 0.0004	< LOD
AWPNB	< LOD	1.38±0.0 3	< LOD	< LOD	< LOD	0.0025± 0.0007	0.0012± 0.0010	0.0010± 0.0004	0.0087± 0.0009	0.0010± 0.0008

*LOD: Low detected Density

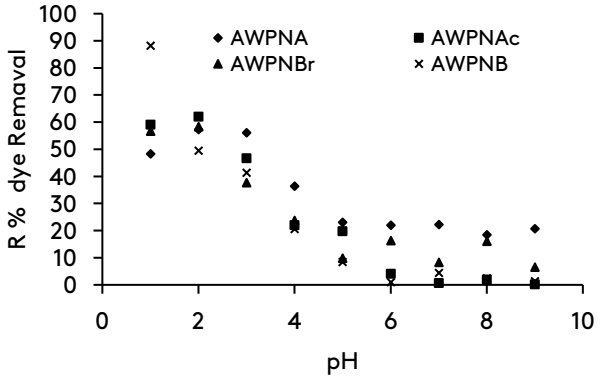

Fig.4. Effect of pH of solution on Bemacid Red dye removal.

3.3. Effect of contact time in Bemacid Red dye removal

The effect of contact time in Bemacid Red dye removal is presented in Figure 5. Through this presentation, it is clear that to distribute the dye adsorption kinetics in three steps, fast step just for the first 5 minute (Step 1) where all the active sites are free and able to fix anionic dye group, following by medium step from 5min to 25min (Step 2) Here the number of active sites is reduced and it is normal that the fixed dye amount decreases and the last step is the slowest, this is the equilibrium step (Step 3), in this step almost all active sites are occupied by dye anionic groups. The kinetic is fast and the balance is reached in the 40 minutes. The optimum time value for the others tests is 40 min. Through the obtained results, the time effect on the efficiency of the various used adsorbents is positive, the same observations are found by Sedigheh [30] during the decomposition of methylene blue using ZnO-SnO_2 as catalyst. The present results are in accordance with the previously reported results [31-36].

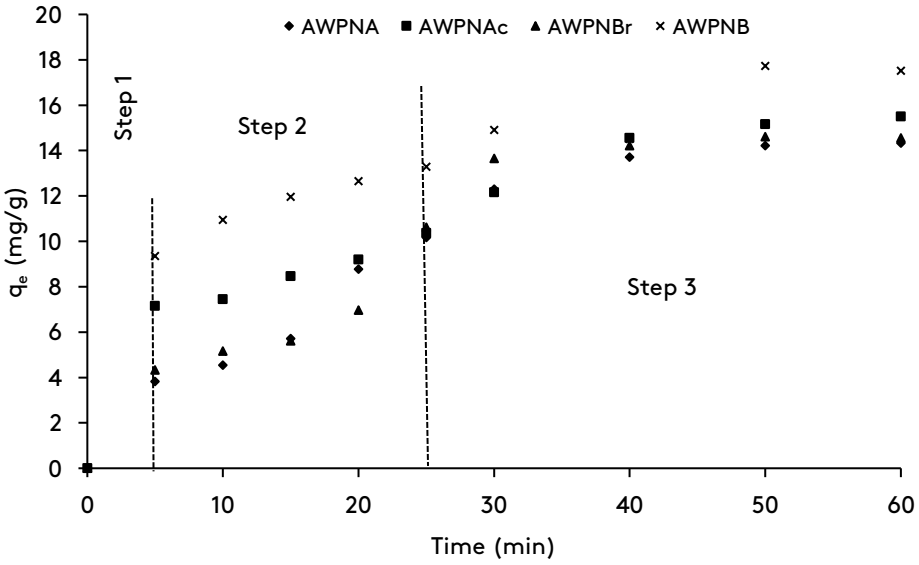

Fig.5. Effect of contact time on Bemacid Red dye removal.

3.4. Effect of initial dye concentration in Bemacid Red dye removal

The fixed dye amount of the four support increases with increase in initial dye concentration and remained nearly constant after the equilibrium time. Where adsorption capacity for Bemacid Red increased from 9 mg/g to 128 mg/g, from 7 mg/g to 113 mg/g, from 6 mg/g to 103 mg/g and from 5 mg/g to 95 mg/g when the initial dye concentration pass from 10 mg/L to 800 mg/L when AWPNB, AWPNBr, AWPNAc and AWPNA respectively are used as adsorbents. The maximum adsorption capacity of Bemacid Red dye onto the different adsorbents follows the order q_e(AWPNB)>q_e(AWPNBr)> q_e(AWPNAc)> q_e(AWPNA). All the obtained values of Bemacid Red due adsorption capacity are lower than found by Tarek et al. [37] when they used mandarin peels as an adsorbent to treat Synthetic aromatic Acid Brown (AB14) with q_e = 416 mg/g.

3.5. Effect of temperature in Bemacid Red dye removal

Figure 7 (**a**), (**b**), (**c**), and (**d**) depict the effects of temperature on adsorption capacity of Bemacid Red dye by the different adsorbents. Significant decrease of adsorption capacities of Bemacid Red dye from 147 mg/g to 93.7 mg/g, from 91.2 mg/g to 23.8 mg/g, from 124.3 mg/g to 63.2 mg/g and from 135.4 mg/g to 103 mg/g on AWPNB, AWPNA; AWPNAc and AWPNBr respectively, indicates the exothermic nature of the process. The same trend was also observed for Bemacid Red adsorption onto brewery waste [19]. Physically at higher temperatures the mobility of molecules increases, which leads to an increase in increased collision and a bond of molecules with the adsorption sites on the other hand in our case the increase in temperature destroys the already trained bonds between the dye molecules and the adsorption sites on different biomass. The same trend was observed during the adsorption of Methylene blue dye onto sulfuric acid–treated orange peel studied by Tarek et al. [37]. From the obtained results of the Batch study, the studied parameters affected the adsorption capacities of different adsorbents in a positive way, the case of: contact time and initial dye concentration, or negative way as the case of: pH solution and temperature. The optimum parameters of the Bemacid Red dye adsorption are: pH =1, t = 40 min, C= 400 mg/L and T = 20 °C for the raw and treated adsorbents. Also from the results, the treatment type plays a very important role in the Bemacid Red adsorption. The NaOH treatment adsorbent gives the best values (q_e =136 mg/g) that favor him in front of the other treated adsorbents.

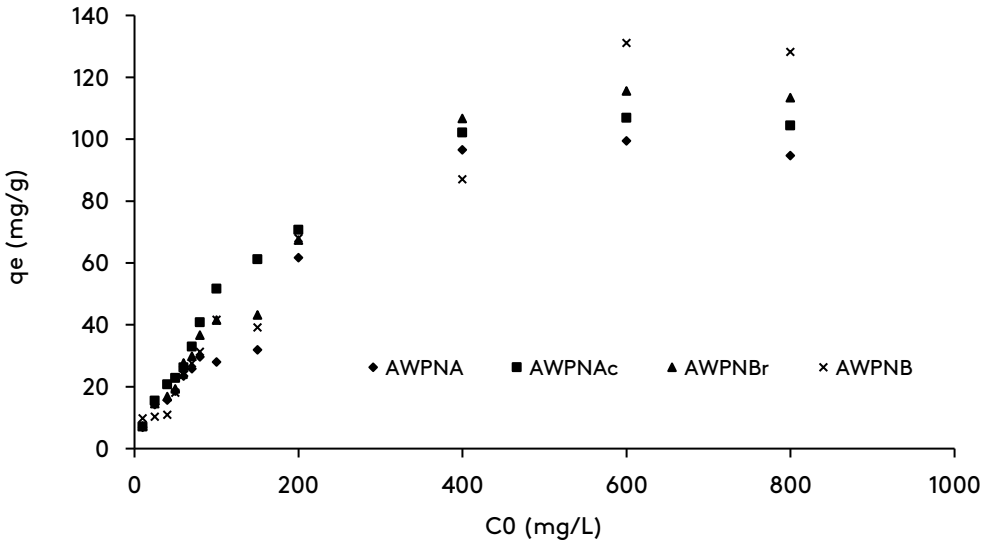

Fig.6. Effect of initial dye concentration on Bemacid Red dye removal.

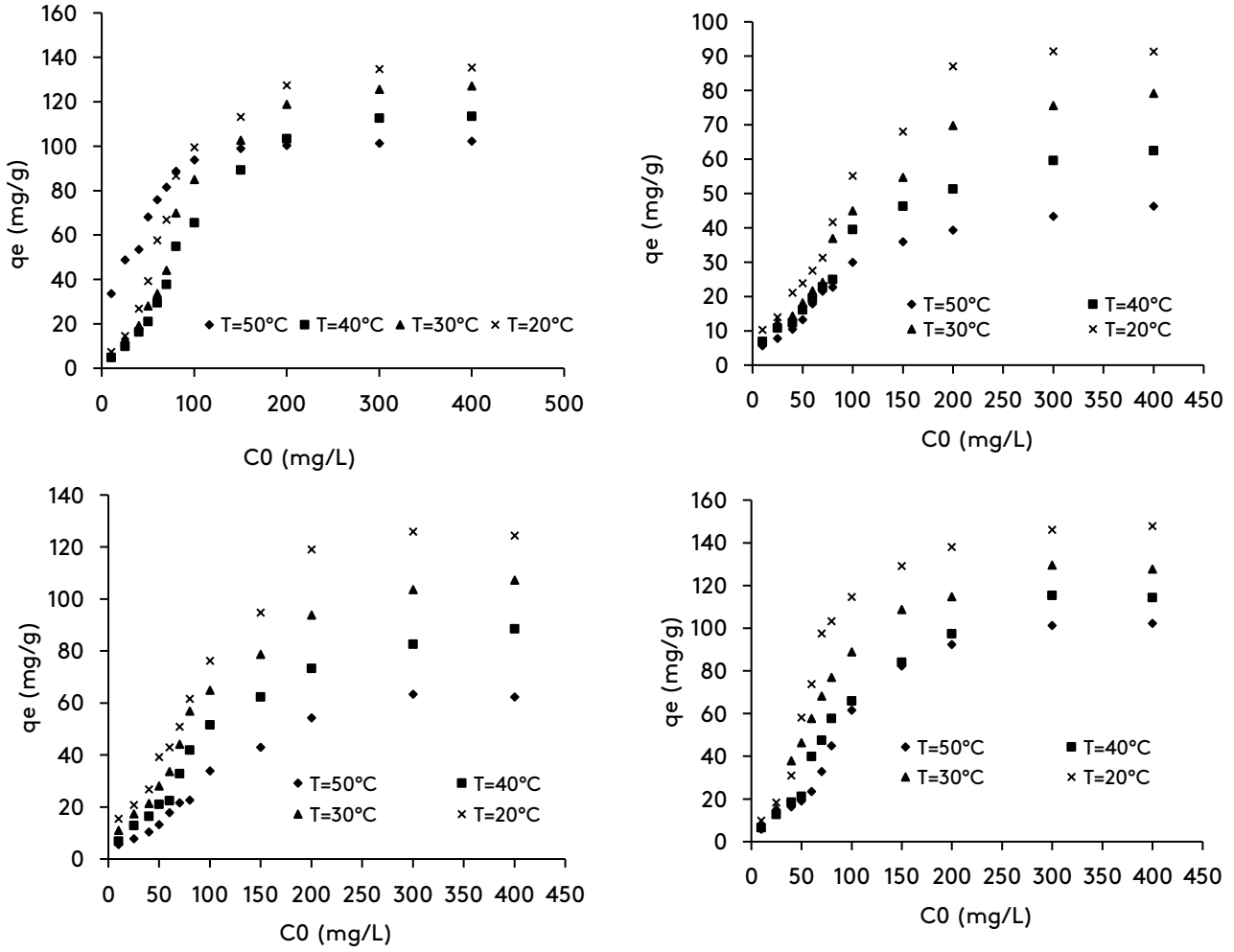

Fig.7. Effect of temperature on Bemacid Red dye removal (a) AWPNBr, (b) AWPNA, (c) AWPNAc and (d) AWPNB.

3.6. Removal of Bemacid Red dye at optimised conditions

The kinetic data of the effect of the contact time study obtained were analyzed according to the classic linear forms of pseudo-first order and pseudo-second order kinetic models to determine the best suited to the results, the kinetic models of pseudo -First order and pseudo-second order are generally expressed as follows [19]:

$$\mathrm{Ln}(q_e - q_t) = \mathrm{Ln}q_e - k_1 t \quad (3)$$

$$\frac{t}{q_t} = \frac{1}{k_2 q_e^2} + \frac{1}{q_e} t \quad (4)$$

Where q_e is the amount of Bemacid Red dye adsorbed per unit mass of adsorbent at equilibrium (mg/g), q_t is the amount of Bemacid Red dye adsorbed per unit mass of adsorbent at any time t (mg/g), t is the time (min), and k_1 and k_2 are the pseudo-first- and second order rate constant (min^{-1} and mg $g^{-1}min^{-1}$) respectively. Figures 8 and 9 represent the two kinetic models, and Table 2 regroups the results of the kinetic study. The calculated q_e values of the pseudo first order kinetic models for all the four adsorbents differ significantly to the experimental q_e values. However, the q_e values estimated in the pseudo-secondary kinetic model were very close to the values of experimental q_e for all tested adsorbents. In addition, the values of determination coefficient (R^2) obtained from the pseudo-second kinetic model are more important than the R^2 values obtained from the pseudo-first kinetic model, and this indicating that the pseudo-secondary kinetic model obeys better with kinetic data adsorption.

Table.2. Kinetic parameters of the pseudo-first and second-order models.

Pseudo-first order kinetic model				
Adsorbents	AWPNB	AWPNBr	AWPNAc	AWPNA
q_{exp}(mg/g)	17.5	14.5	15.5	13.82
k_1 (min^{-1})	0.0596	0.0717	0.0577	0.0591
q_e(mg/g)	15.52	20.21	17.05	19.74
R^2	0.81	0.91	0.95	0.96
Pseudo-second order kinetic model				
k_2 (min.g mg^{-1})	0.009	0.007	0.008	0.009
q_e (mg/g)	17.45	16.28	16.69	15.38
R^2	0.984	0.971	0.980	0.977

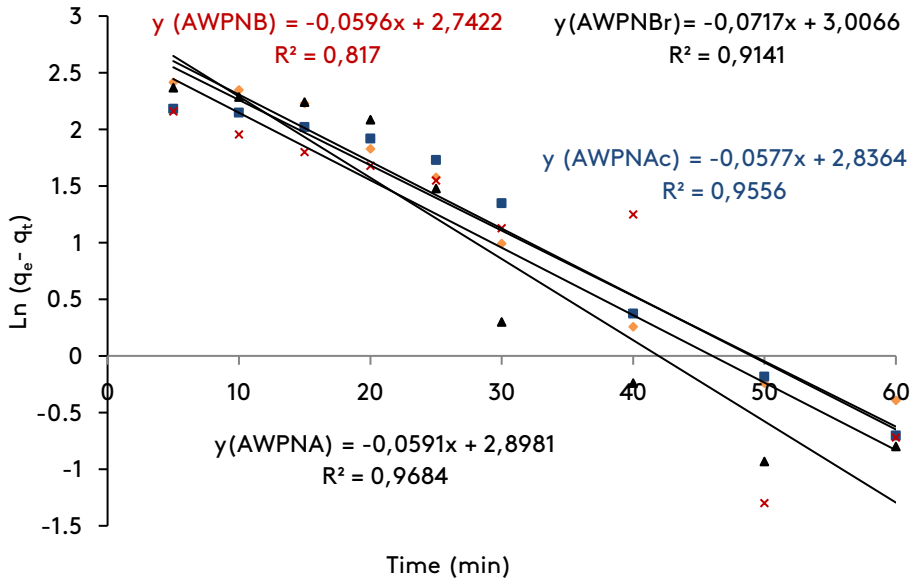

Fig.8. Pseudo-first order kinetic model.

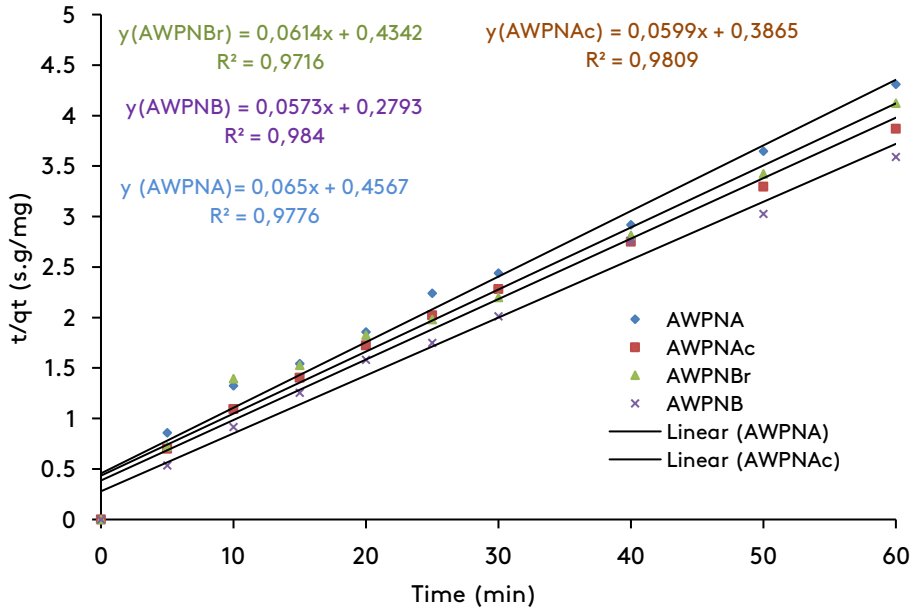

Fig.9. Pseudo-second order kinetic model.

4. Physical description of the Bemacid Red adsorption isotherm

To understand the adsorption isotherm of Bemacid Red dye, theoretical adsorption models derived from statistical physics elements can be used. To this aim, different models can be tested on the experimental data set.

a-Monolayer model with single energy (MLSE)

In this model, the formation of a monolayer on AWPNA, AWPNB, AWPNBr and AWPNAc is realized by direct interactions between the Bemacid Red molecules and the different biomass surface. Under the model hypotheses, one Bemacid Red molecules can be linked by one active site (functional group) of the adsorbents and all the active sites have the same energy level E_1. In this theoretical analysis, the capture number of Bemacid Red molecules was estimated by the n parameter. The equation of this model is [37]:

$$q_e = \frac{nD_m}{1 + \left(\frac{C_{1/2}}{C}\right)^n} \quad (5)$$

Where: D_m represent the density of active groups (mg/g), $C_{1/2}$ is the concentration at half-saturation and C is the Bemacid Red dye concentration. The saturation adsorption capacity q_{sat} in this model was calculated as [37]:

$$q_{sat} = nD_m \text{ (mg/g)} \quad (6)$$

b-Double layer model with two energies (DLMTE)

In this model there is possibility of formation of two layers of Bemacid Red molecules on the different biomass surfaces, the first layer is the result of the interactions between the Bemacid Red molecules and the different biomass surfaces, and the second layer result when there is interaction between the Bemacid Red molecules (Bemacid Red / Bemacid Red). The expression of this model is [38]:

$$q_e = nD_m \frac{\left(\frac{C}{C_1}\right)^n + 2\left(\frac{C}{C_2}\right)^{2n}}{1 + \left(\frac{C}{C_1}\right)^n + \left(\frac{C}{C_2}\right)^{2n}} \quad (7)$$

Where: *n* represent the number of the capture of Bemacid Red molecules, C_1 and C_2 are the two concentrations at half-saturation of the first and second formed layers, respectively. The saturation adsorption q_{sat} in this model was determined as [38]:

$$q_{sat} = 2.n.D_m \text{ (mg/g)} \quad (8)$$

n order to modeling the experimental adsorption isotherms of Bemacid Red on AWPNA, AWPNB, AWPNBr and AWPNAc, the MLSE and DLMTE models were applied.

4.1. Description of the adsorption mechanism according to the adequate model

Multivariable non –linear regression method was used to adjust the different parameters of the two statistical physics models to the experimental isotherms data. Also, another method was utilized to select the best model, the damped least-squares (DLS) method which is based on the determination of estimated standard error (root mean square error RMSE). The values of the *RMSE* and determination coefficient R^2 were necessary to select the best model. The comparison of the different values of *RMSE* and R^2 was applies to select one of the two physics MLSE and DLMTE models which fit the dye adsorption isotherms data onto the different types of raw and treated adsorbents. Each parameter of the two physics models can be used to interpret theoretically the dye adsorption mechanism. All experimental isotherms data were fitted using the two cited analytical models (MLSE and DLMTE). The Table.3 represents the different parameters of monolayer with single energy for different biomass and temperature. From the depicts values, the variation domains of determination coefficient R^2 is from 0.898 to 0.999 for the different adsorbents, which is conform to the obtained results by the study of CO_2 adsorption onto ZSM-5 zeolite where the range was from 0.791 to 0.982 [39] when the temperature increases from 293 to 323 K. Indeed, the estimated results of different parameters by the monolayer model (MLSE) show that this model is not acceptable to express the Bemacid Red dye adsorption mechanism, from the Table.3 and for certain temperature value, the value of Bemacid Red dye adsorption capacity are not compatible with experimental results. Therefore, this model is inappropriate to describe the Bemacid Red dye adsorption. Regarding the double layer model (Table.4), the correlation coefficients R^2 values are close to the unity (from 0.985 to 0.99), small values for *RMSE* compared to obtained values for MLSE model. In addition we can notice that the adjusted parameters values are reasonable compared to the experimental values. Therefore, this model can be

acceptable to supply reasonable study to the Bemacid Red dye adsorption. The obtained values are in accordance with previously obtained results [38-39].

Table.3. Parameters of the monolayer model MLSE.

	T(K)	n	D_m	q_{sat} (mg/g)	$C_{1/2}$	R^2	RMSE
AWPNB	293	1.708	93.741	160.194	11.236	0.995	12.244
	303	0.265	2679.52	710.072	59299	0.967	8.955
	313	5.693	16.844	95.904	40.284	0.999	4.967
	323	1.452	85.109	123.116	39.748	0.999	2.379
AWPNBr	293	1.981	72.625	143.885	52.774	0.992	15.761
	303	1.378	113.728	156.807	66.847	0.993	7.035
	313	2.168	56.984	123.553	58.873	0.993	3.876
	323	1.509	91.745	138.534	96.369	0.997	6.975
AWPNAc	293	1.735	62.732	108.872	25.780	0.999	14.380
	303	1.661	66.003	109.696	36.870	0.999	2.683
	313	1.994	46.202	92.152	54.902	0.999	3.236
	323	1.800	38.314	68.973	75.479	0.985	2.602
AWPNA	293	5.609	20.179	113.205	29.092	0.996	16.515
	303	1.355	31.487	42.668	33.776	0.938	3.457
	313	1.119	26.286	29.436	21.701	0.898	2.628
	323	2.42	10.081	24.437	28.218	0.918	2.618

Table.4. Parameters of the double layer model DLMTE.

	T(K)	n	D_m	q_{sat} (mg/g)	C_1	C_2	R^2	RMSE
AWPNB	293	0.419	311.001	261.176	20.001	107.000	0.991	7.193
	303	1.160	86.369	200.376	17.321	100.476	0.996	9.290
	313	3.122	15.693	98.006	42.705	37.979	0.994	4.580
	323	1.041	127.012	246.686	57.132	106.001	0.999	5.092
AWPNBr	293	0.442	98.537	87.236	26.388	129.948	0.992	4.991
	303	1.050	73.690	154.76	74.719	64.842	0.997	2.914
	313	1.573	39.641	124.786	66.141	59.561	0.999	0.954
	323	2.716	19.489	105.902	49.684	58.779	0.998	1.351
AWPNAc	293	0.551	257.258	283.898	130.124	270.138	0.998	2.002
	303	0.384	129.308	99.528	507.583	18.967	0.998	1.781
	313	1.691	22.193	75.094	43.584	38.199	0.998	1.330
	323	8.267	2.003	33.127	0.779	8.732	0.985	12.448
AWPNA	293	5.921	6.847	81.096	6.038	20.201	0.990	5.203
	303	1.069	20.576	44.026	24.511	35.197	0.994	1.145
	313	0.514	4.305	4.426	2.169	46.731	0.995	0.674
	323	0.389	54.133	42.164	90.964	61.289	0.996	0.504

4.2. Analysis of Steric parameter 'n' number of linked dye molecules onto sites surface

Through the '*n*' values, we try to provide idea about the adsorption mechanism, the distribution position or orientation and the degree of aggregation of Bemacid Red dye ions on the surface of the different adsorbents. From the literature, the '*n*' value gives three possibilities, (i) when $n < 0.5$, the active group adsorbs a portion of dye molecule per site with parallel adsorption orientation and multi-bonding adsorption mechanism, (ii) for $0.5 < n < 1$ the molecule dye adsorption is carried out by two types orientation non -parallel and parallel in same time with different percentages, (iii) $n > 1$ Adsorption mechanism is multi-molecular in this case the active group accepts one or more dye molecules, with a non -parallel orientation [39]. All the obtained statistical results are in accordance with

the results of previous researches [35-37]. The formula used to calculate 'n' is [39]:

$$n=x+(1-x).2 \quad (9)$$

Form this equation there is possibility to determine the percentage of each position orientation, where, (x) represent the percentage of active groups occupied by one dye molecule and (1-x) depicts the percentage of sites occupied by two molecules. Figure 10 depicts the variation of the linked dye molecules number onto the different adsorbent. It is clear to observe that the behavior of the n variation for acidic treatment adsorbent (AWPNA) is inversely that observed in the case of raw adsorbent (AWPNBr).

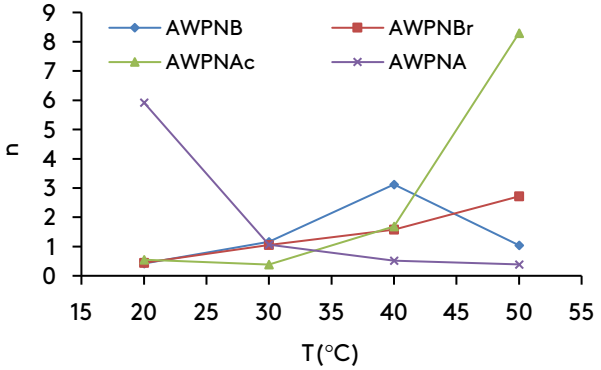

Fig. 10. Effect of temperature on Bemacid Red-ETL captured molecules number per site.

The n value variation domains for raw adsorbent (AWPNB) and basic treatment adsorbent (AWPNBr) are the same: from 0.419 to 3.122 and from 0.442 to 2.716 for AWPNB and AWPNBr respectively. The behavior of the n value variation of the acidic treatment adsorbent is unique where n values decrease when temperature increases. Also from Table.4, it is clear to reveal that two cases for n values can take place in Bemacid Red dye adsorption onto the raw and treated adsorbent system. The '*n*' values lower than 0.5 is observed at lower temperature (25 °C) for AWPNB and AWPNBr adsorbents and at high temperature (50 °C) for acidic treatment adsorbent (AWPNA). These results indicate that Bemacid Red dye molecules are fixed onto receptor sites via one type orientation (parallel orientation). When the temperature passes from 30°C to 50°C, all the *n* values of AWPNB and AWPNBr adsorbents are greater than one, so the active groups accept one or more of Bemacid Red dye molecules and showing non-parallel orientation. The lowest and highest values of n are observed in the case of organic treatment adsorbent of 0.384 and 8.267 respectively. So using the Eq. (9) for the case of n =1.691, the occupation percentage of each site was: n=1.691= x+ (1-x).2 reveals that 30.9% of sites are occupied by one Bemacid Red dye molecule and 69.1% of sites are occupied by two molecules in the case of AWPNAc. The different in the behavior of n values indicate the effect of treatment in the active sites of the different surface adsorbents. The same range of variation is found by others researches [38-40].

4.3. Density of linking active groups D_m

The Figure 11 depicts the variation of density of linking active groups as function to variation of temperature end different adsorbent. The results show that the maximal density value of the Bemacid Red dye, which is 311mg.g^{-1}, is recorded during the treatment with AWPNB adsorbent. This gives idea that the type of treatment contributes in a remarkable way in order to activate or deactivate accessible adsorption active groups and therefore regenerates a steric obstacle in these active groups. It is clear to conclude that the type of treatment manages the adsorption capacity value. The same observations are reported in previous studies [37-38].

4.4. Adsorption capacity at saturation q_{sat}

The value of the adsorption capacity to saturation in the two MLSE and DLMTE models depends on the value of the two steric '*n*' and 'D_m' parameters. The depict values in Table.4 (and in Figure 12) indicate that the behavior of the adsorption capacity at the saturation can followed the next trend: q_{sat} (AWPNB) > q_{sat} (AWPNBr) > q_{sat} (AWPNA) at the same temperature in general. These results indicate that the biomass AWPNB present a high affinity towards the Bemacid Red dye compared to the other adsorbent. The same observations are recorded in the discussion of the first results of this study. The q_{sat} behavior when the AWPNAc is used as adsorbent is different from that saved for other adsorbents, where the maximum value of q_{sat} which is 283 mg/g is recorded, and also through the Table .4 is observed that there is a decrease of the value of q_{sat} with increase in temperature and it is the only one comprehensive which describes in a closer way the adsorption of the color Bemacid Red

and indicate the exothermic character of the Bemacid Red dye adsorption. The same variations of these statistical parameters are observed by Bouaziz et al. [41].

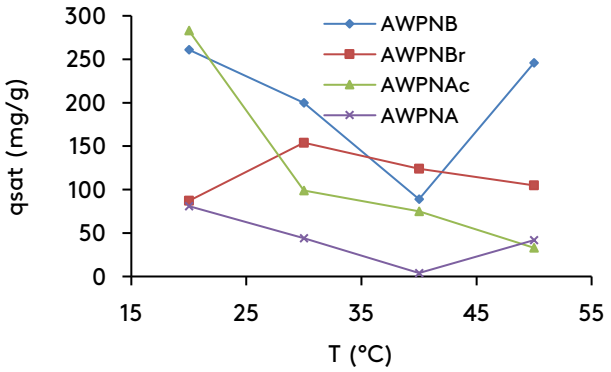

Fig.12. Effect of temperature on Adsorption capacity at saturation.

5. Conclusions

In this research, the experimental data of Bemacid Red dye adsorption onto raw and treated Avokado adsorbent are analyzed in a kinetic and theoretical physics way. The kinetic pseudo second order fit well with the kinetics data. The contact time and initial due concentration have positive effect on the Bemacid Red dye adsorption capacity. However, the pH medium and the temperature have negative effects on the Bemacid Red dye removal. The double layer with two energies from the theoretical physics models manage the isotherm data and interpret the Bemacid Red dye adsorption mechanism. From the steric parameters, the active groups accept parallel Bemacid Red dye molecules orientation when temperature is lower (n<0.5), and non-parallel orientation when temperature is higher (n>1). The basic treatment gives an important affinity towards Bemacid Red dye compared to the other treatments.

Abbreviations Table

AWPN	Avokado waste peel/nut
AWPNA	Avokado waste peel/nut Acidic treatment
AWPNAc	Avokado waste peel/nut Acetone treatment
AWPNB	Avokado waste peel/nut Basic treatment
AWPNBr	Raw Avokado waste peel/nut
C_1	Concentrations at half-saturation of the first layer
C_2	Concentrations at half-saturation of the second layer
DLMTE	Double layer model with two energies
DLS	Damped least-squares
D_m	Density of linking groups
MLSE	Monolayer model with single energy
n	Number of dye molecules
q_{sat}	Adsorption capacity at saturation
RMSE	Root mean square error
x	Percentage of occupied active groups

Acknowledgments

The authors express their gratitude to team of Analytical Chemistry–Laboratory of Valencia University- for their help in carrying out sample analysis.

References

[1] van Vliet, M. T., Jones, E. R., Flörke, M., Franssen, W. H., Hanasaki, N., Wada, Y., Yearsley, J. R. (2021). Global water scarcity including surface water quality and expansions of clean water technologies. *Environmental research letters*, *16*(2), 024020.

[2] Abbas, M., Harrache, Z., Trari, M. (2020). Mass-transfer processes in the adsorption of crystal violet by activated carbon derived from pomegranate peels: kinetics and thermodynamic studies. *Journal of engineered fibers and fabrics*, *15*, 1558925020919847.

[3] Gómez-Avilés, A., Sellaoui, L., Badawi, M., Bonilla-Petriciolet, A., Bedia, J., Belver, C. (2021). Simultaneous adsorption of acetaminophen, diclofenac and tetracycline by organo-sepiolite: experiments and statistical physics modelling. *Chemical engineering journal*, *404*, 126601.

[4] Adamu, A., Zewge, F., Chebude, Y. (2022). Valorization of spent coffee grounds through pyrolysis as adsorbent for the removal of Vivizole Red 3BS dye from aqueous solution. *Water practice and technology*, *17*(5), 1019-1034.

[5] Donkadokula, N. Y., Kola, A. K., Naz, I., Saroj, D. (2020). A review on advanced physico-chemical and biological textile dye wastewater treatment techniques. *Reviews in environmental science and bio/technology*, *19*(3), 543-560.

[6] El Hanandeh, A., Mahdi, Z., Imtiaz, M. S. (2021). Modelling of the adsorption of Pb, Cu and Ni

ions from single and multi-component aqueous solutions by date seed derived biochar: Comparison of six machine learning approaches. *Environmental research*, *192*, 110338.

[7] Gul Zaman, H., Baloo, L., Pendyala, R., Singa, P. K., Ilyas, S. U., Kutty, S. R. M. (2021). Produced water treatment with conventional adsorbents and MOF as an alternative: A review. *Materials*, *14*(24), 7607.

[8] Abbasi, S., Dastan, D., Ţălu, Ş., Tahir, M. B., Elias, M., Tao, L., Li, Z. (2022). Evaluation of the dependence of methyl orange organic pollutant removal rate on the amount of titanium dioxide nanoparticles in MWCNTs-TiO_2 photocatalyst using statistical methods and Duncan's multiple range test. *International journal of environmental analytical chemistry*, 1-15.

[9] Abbasi, S., Ahmadpoor, F., Imani, M., Ekrami-Kakhki, M. S. (2020). Synthesis of magnetic Fe_3O_4@ ZnO@ graphene oxide nanocomposite for photodegradation of organic dye pollutant. *International journal of environmental analytical chemistry*, *100*(2), 225-240.

[10] Abbasi, S., Hasanpour, M., Ahmadpoor, F., Sillanpää, M., Dastan, D., Achour, A. (2021). Application of the statistical analysis methodology for photodegradation of methyl orange using a new nanocomposite containing modified TiO_2 semiconductor with SnO_2. *International journal of environmental analytical chemistry*, *101*(2), 208-224.

[11] Abbasi, S. (2020). Adsorption of dye organic pollutant using magnetic ZnO embedded on the surface of graphene oxide. *Journal of inorganic and organometallic polymers and materials*, *30*(6), 1924-1934.

[12] Abbasi, S. (2022). The degradation rate study of Methyl Orange Using MWCNTs@ TiO_2 as photocatalyst, Application of statistical analysis based on Fisher's F distribution. *Journal of cluster science*, *33*(2), 593-602.

[13] Abbasi, S. (2018). Investigation of the enhancement and optimization of the photocatalytic activity of modified TiO_2 nanoparticles with SnO_2 nanoparticles using statistical method. *Materials research express*, *5*(6), 066302.

[14] Torres, E. (2020). Biosorption: A review of the latest advances. *Processes*, *8*(12), 1584.

[15] Ahmad, T., Danish, M. (2022). A review of avocado waste-derived adsorbents: Characterizations, adsorption characteristics, and surface mechanism. *Chemosphere*, 134036.

[16] Elizalde-González, M. P., Mattusch, J., Peláez-Cid, A. A., Wennrich, R. (2007). Characterization of adsorbent materials prepared from avocado kernel seeds: Natural, activated and carbonized forms. *Journal of analytical and applied pyrolysis*, *78*(1), 185-193.

[17] Un, U. T., Ates, F., Erginel, N., Ozcan, O., Oduncu, E. (2015). Adsorption of Disperse Orange 30 dye onto activated carbon derived from holm oak (Quercus ilex) acorns: A 3k factorial design and analysis. *Journal of environmental management*, *155*, 89-96.

[18] Gatabi, M. P., Moghaddam, H. M., Ghorbani, M. (2016). Point of zero charge of maghemite decorated multiwalled carbon nanotubes fabricated by chemical precipitation method. *Journal of molecular liquids*, *216*, 117-125.

[19] Ouazani, F., Iddou, A., Aziz, A. (2017). Biosorption of Bemacid Red dye by brewery waste using single and poly-parametric study. *Desalination and water treatment*, *93*, 171-179.

[20] Al-Zawahreh, K., Barral, M. T., Al-Degs, Y., Paradelo, R. (2021). Comparison of the sorption capacity of basic, acid, direct and reactive dyes by compost in batch conditions. *Journal of environmental management*, *294*, 113005.

[21] Abbasi, S., Hasanpour, M. (2017). The effect of pH on the photocatalytic degradation of methyl orange using decorated ZnO nanoparticles with SnO_2 nanoparticles. *Journal of materials science: Materials in electronics*, *28*(2), 1307-1314.

[22] Abbasi, S., Hasanpour, M. (2017). Variation of the photocatalytic performance of decorated MWCNTs (MWCNTs-ZnO) with pH for photo degradation of methyl orange. *Journal of materials science: materials in electronics*, *28*(16), 11846-11855.

[23] Abbasi, S. (2021). Improvement of photocatalytic decomposition of methyl orange by modified MWCNTs, prediction of

degradation rate using statistical models. *Journal of materials science: Materials in electronics*, *32*(11), 14137-14148.

[24] Abbasi, S. (2021). Response surface methodology for photo degradation of methyl orange using magnetic nanocomposites containing zinc oxide. *Journal of cluster science*, *32*(4), 805-812.

[25] Abbasi, S., Ekrami-Kakhki, M. S., Tahari, M. (2017). Modeling and predicting the photodecomposition of methylene blue via ZnO–SnO_2 hybrids using design of experiments (DOE). *Journal of materials science: materials in electronics*, *28*(20), 15306-15312.

[26] Roozban, N., Abbasi, S., Ghazizadeh, M. (2017). Statistical analysis of the photocatalytic activity of decorated multi-walled carbon nanotubes with ZnO nanoparticles. *Journal of materials science: Materials in electronics*, *28*(8), 6047-6055.

[27] Abbasi, S., Ekrami-Kakhki, M. S., Tahari, M. (2019). The influence of ZnO nanoparticles amount on the optimisation of photo degradation of methyl orange using decorated MWCNTs. *Progress in industrial ecology, an international journal*, *13*(1), 3-15.

[28] Abbasi, S. (2019). Photocatalytic activity study of coated anatase-rutile titania nanoparticles with nanocrystalline tin dioxide based on the statistical analysis. *Environmental monitoring and assessment*, *191*(4), 1-13.

[29] Roozban, N., Abbasi, S., Ghazizadeh, M. (2017). The experimental and statistical investigation of the photo degradation of methyl orange using modified MWCNTs with different amount of ZnO nanoparticles. *Journal of materials science: Materials in electronics*, *28*(10), 7343-7352.

[30] Abbasi, S., Hasanpour, M., Ekrami-Kakhki, M. S. (2017). Removal efficiency optimization of organic pollutant (methylene blue) with modified multi-walled carbon nanotubes using design of experiments (DOE). *Journal of materials science: Materials in electronics*, *28*(13), 9900-9910.

[31] Farooq, M. U., Jalees, M. I., Iqbal, A., Zahra, N., Kiran, A. (2019). Characterization and adsorption study of biosorbents for the removal of basic cationic dye: kinetic and isotherm analysis. *Desalin water treat*, *160*, 333-342.

[32] Arulkumar, M., Sathishkumar, P., Palvannan, T. (2011). Optimization of Orange G dye adsorption by activated carbon of Thespesia populnea pods using response surface methodology. *Journal of hazardous materials*, *186*(1), 827-834.

[33] Wekoye, J. N., Wanyonyi, W. C., Wangila, P. T., Tonui, M. K. (2020). Kinetic and equilibrium studies of Congo red dye adsorption on cabbage waste powder. *Environmental chemistry and ecotoxicology*, *2*, 24-31.

[34] Kapoor, R. T., Rafatullah, M., Siddiqui, M. R., Khan, M. A., Sillanpää, M. (2022). Removal of reactive black 5 dye by banana peel biochar and evaluation of Its phytotoxicity on tomato. *Sustainability*, *14*(7), 4176.

[35] Lafi, R., Montasser, I., Hafiane, A. (2019). Adsorption of congo red dye from aqueous solutions by prepared activated carbon with oxygen-containing functional groups and its regeneration. *Adsorption science and technology*, *37*(1-2), 160-181.

[36] Asuquo, E. D., Martin, A. D., Nzerem, P. (2018). Evaluation of Cd (II) ion removal from aqueous solution by a low-cost adsorbent prepared from white yam (Dioscorea rotundata) waste using batch sorption. *ChemEngineering*, *2*(3), 35.

[37] Eldeeb, T. M., Aigbe, U. O., Ukhurebor, K. E., Onyancha, R. B., El-Nemr, M. A., Hassaan, M. A., El Nemr, A. (2022). Biosorption of acid brown 14 dye to mandarin-CO-TETA derived from mandarin peels. *Biomass conversion and biorefinery*, 1-21.

[38] Senthil Kumar, P., Fernando, P. S. A., Ahmed, R. T., Srinath, R., Priyadharshini, M., Vignesh, A. M., Thanjiappan, A. (2014). Effect of temperature on the adsorption of methylene blue dye onto sulfuric acid–treated orange peel. *Chemical engineering communications*, *201*(11), 1526-1547.

[39] Aouaini, F., Bouaziz, N., Khemiri, N., Alyoussef, H., Nasr, S., Ben Lamine, A. (2022). Adsorption of methyl orange, acid chrome blue K, and Congo red dyes on MIL-101-NH2 adsorbent: Analytical interpretation via advanced model. *AIP advances*, *12*(3), 035307.

[40] Hanafy, H., Li, Z., Sellaoui, L., Yazidi, A., Wang, H., Lima, E. C., Erto, A. (2021). Theoretical interpretation of the adsorption of amoxicillin on activated carbon via physical model. *Environmental science and pollution research*, *28*(24), 30714-30721.

[41] Bouaziz, N., Ben Manaa, M., Bouzid, M., Ben Lamine, A. (2020). Adsorption of hydrogen in defective carbon nanotube: modelling and consequent investigations using statistical physics formalism. *Molecular physics*, *118*(3), e1606460.